Modeling of Olsen cycle for pyroelectric energy harvesting and assessment of abnormal electrocaloric effect in ferroelectric single crystals

Gaspard Taxil, Mickaël Lallart, Benjamin Ducharne, T T Nguyen, H. Kuwano, T. Ono, Gaël Sebald

Modeling of Olsen cycle for pyroelectric energy harvesting and assessment of abnormal electrocaloric effect in ferroelectric single crystals

G. Taxil,[1,2,3,4] M. Lallart,[1] B. Ducharne,[1,2] T. T. Nguyen,[2,4] H. Kuwano,[2,4] T. Ono,[3] and G. Sebald[1,2]

[1)] *Univ. Lyon, INSA-Lyon, LGEF EA682, F-69621, France.*

[2)] *ELyTMaX IRL 3757, CNRS, Univ. Lyon, INSA Lyon, Centrale Lyon, Université Claude Bernard Lyon 1, Tohoku University, Sendai, Japan.*

[3)] *Graduate School of Engineering, Tohoku University, Sendai 9808579, Japan.*

[4)] *New Industry Creation Hatchery Center (NICHe), Tohoku University, 6-6-10 Aramaki-Aoba, Aoba-ku Sendai, Miyagi 980-8579, Japan.*

(*Electronic mail: mickael.lallart@insa-lyon.fr)

(*Electronic mail: gaspard.taxil@insa-lyon.fr)

(Dated: 2 November 2022)

The energy conversion potential of ferroelectric materials originating from their phase transitions in particular temperature ranges and electric field values is very promising. Pyroelectric energy harvesting consists in directly converting thermal energy into electrical one. Due to its high energy conversion potential, the Olsen cycle is the most favorable for pyroelectric energy harvesting. This cycle includes two isothermal and two constant electric field branches. In this study, the Olsen cycle was modeled, then varying temperatures and applied electric field directions for different crystal orientations were simulated. Polarization responses were obtained via the Landau-Devonshire theory. Then, an innovative way to model the electrocaloric effect was proposed; experimental results and first-principle calculations confirmed the simulation results. The resulting negative electrocaloric effect due to crystal orientation, previously reported in the literature, has been successfully simulated through a phenomenological approach. Finally, we identified which phase transitions are interesting for pyroelectric energy harvesting applications depending on crystal orientations while obtaining an energy density in the order of $\approx 10^2 mJ/cm^3$. This value corresponds to previous results in the literature.

I. INTRODUCTION

Energy harvesting from residual energy in the environment is a promising way to power wireless sensors or other low-power devices in harsh or remote conditions. The advantages of this method are the low cost and the absence of maintenance like replacement of batteries (for instance due to their self-discharge). There has been thus a significant growth of studies in energy harvesting in the last decades due to the spread of the "Internet of Things" (IoT), which implies the connection of many low-powered connected devices autonomously exchanging data. There are several types of energies in the environment that can be converted into electrical energy, for instance vibration, solar radiation, wind and waste heat. Waste heat is an underestimated energy source seldomly exploited. Approximately two-thirds of the energy produced in the U.S is rejected as wasted heat[1]. There are numerous heat sources where energy is produced, including power plants and oil refineries. Other heat sources in daily life are available, including hot water and exhaust pipes. Other growing activities such as the heat dissipated from data centers and solar panels are exciting sources for thermal energy harvesting[2]. Another example is the heat dissipated by the human body[3]or the thermal gradient generated by solar radiations[4] which was used for pyroelectric energy harvesting. The energy challenges of the next decades have increased the interest in waste-heat energy harvesting and different approaches have been developed to take advantage of these energy losses with pyroelectric materials[5]. As for any energy source, one of the significant issues in heat energy harvesting is the low output power. Different methods exist to improve it, like the design of innovative electrical circuits[6,7].The possibility of working on the electromechanical structure with different geometries can also be envisaged[8,9]. Another option is to exploit the phase transitions of ferroelectric materials, but very few studies were dedicated to this approach for energy harvesting[10,11].

Ferroelectric materials are of great interest for a panel of applications such as wireless sensors, memories, transducers and so on. Their capability to convert vibration and temperature into an electrical signal (and conversely) is the most attractive feature of these materials. One of their remarkable properties is also their successive phase transitions either with temperature, applied stress or electric field. While very few studies proposed to take advantage of such transitions, this work aims at using them for energy harvesting purpose. As a first step, the work reported here proposes a thermodynamic phenomenological approach to describe such phase transitions. One significant advantage in using phase transitions in ferroelectric materials is to take benefit of the non-linear response of the polarization close to the transition and thus, increase the polarization variation. The main ferroelectric material used for such an application and studied both theoretically and experimentally is the perovskite structure ABO_3. In the perovskite structure the ferroelectric distorsion gives a relative displacement of the cation with respect to the anion which induces a net polarization. Some perovskite structures such as $BaTiO_3$, $KNbO_3$ (KNO) and $KTa_xNb_{1-x}O_3$ (KTN) undergo three phase transitions from rhombohedral to orthorhombic, from orthorhombic to tetragonal and from tetragonal to cubic with temperature (the symmetry of the crystal increases with temperature), pressure or electric field. The mechanism of

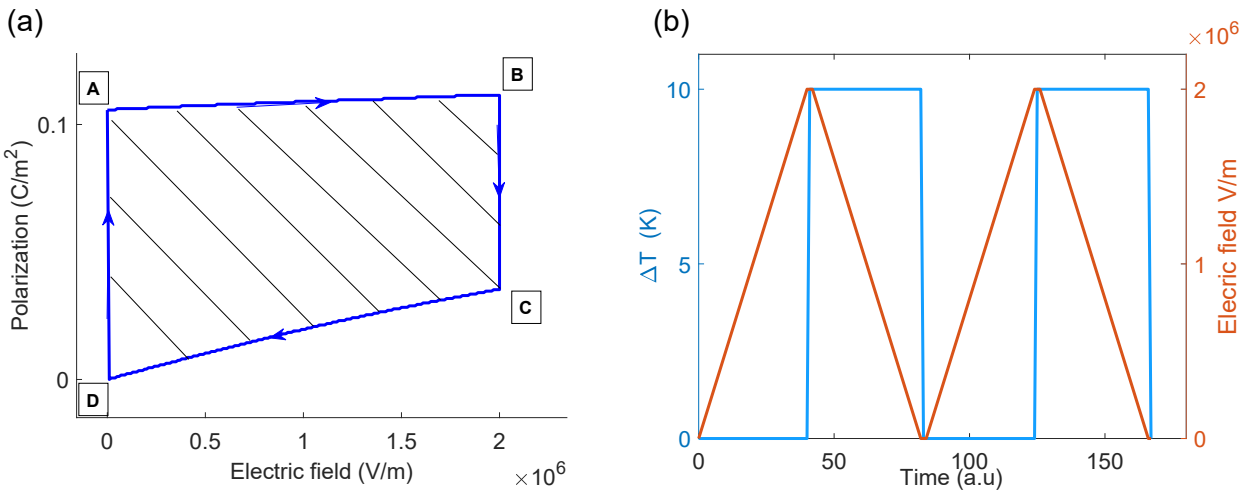

FIG. 1. (a) Representation of a P(E) cycle with the different steps of the Olsen cycle detailed; (b) Evolution of the temperature and the electric field in function of time for two consecutive Olsen cycles in the case of $T_h - T_l = 10K$, $E_i = 0kV/mm$ and $E_f = 2kV/mm$.

phase transitions is very complex and only few theories allow describe them. Among them, the renormalization group works very well but is very complex in its formalism[12]. An easier way relies on the mean-field approximation. However, close to the transitions, this approximation fails to describe properly experimental observations. Hopefully in ferroelectric materials, the nature of the transition allows describing them in the frame of Landau theory (mean field approximation) due to their long-range interactions[13]. For ferroelectrics, Devonshire used in the 1950's the Landau theory to describe the phase transitions of barium titanate[14]. This theory is known as Landau-Devonshire theory and consists of developing the free energy term in power expansion of an order parameter which is the polarization in the case of a ferroelectric materials. In this context, the presents work proposes a comparative study of different ferroelectric materials with perovskite structure for pyroelectric energy harvesting. In a first step, the study will focus on the Olsen cycle and its description. Then, the theoretical approach for different crystal orientations with the Landau-Devonshire theory is explained. After that, the experimental confirmation of the modeling is made with analogy between harvested energy and the electrocaloric effect for different crystallographic orientations of PMN-30PT and $BaTiO_3$. Finally, the best phase transitions of ferroelectric materials for energy harvesting depending on crystal orientations are identified.

II. OLSEN'S CYCLE

Pyroelectric energy harvesting generally uses closed thermodynamic cycles to reach more energy output. Pyroelectric energy harvesting implies thermodynamic cycles in the polarization-electric field space, and in the entropy-temperature space. We can consider the polarization P as the conjugated variable of the electric field E because of the high relative dielectric permittivity $\varepsilon_r >> 1$ for pyroelectrics. Different cycles have been used for pyroelectric energy harvesting[15]. We can quote the Stirling cycle which consists of two isothermal and two constant electric induction processes. Another promising cycle is called the Olsen cycle and it is the one we choose to model here due to its high energy conversion capabilities. The Olsen cycle[15] consists of two isothermal and two constant electric field processes. The cycle starts from a low temperature T_l and an initial electric field E_i. An electric field is applied until a final value E_f (A-B path on Fig. 1(a)). Then, the temperature is increased to a higher value T_h (B-C path). Afterwards, the electric field is decreased to its initial value E_i (C-D path). Finally, the temperature is decreased down to the initial T_l value (D-A path). Previous studies have demonstrated the feasibility and possible future applications of pyroelectric energy harvesting via Olsen cycles[16,17]as waste-heat energy harvesting is a probable hot upcoming topic. In particular, Hanrahan *et al*[16]realized Olsen cycles with a laser-based pyroelectric harvester with a square temperature variation and a triangle function evolution of the electric field. We decided to use this temporal profile in our simulation for preliminary comparison purposes and model assessment. An illustration of the evolution of the temperature and the electric field in our theoretical approach is given in Fig. 4(b). It can be noted that the choice of the functions in a real experiment impacts the output energy[18]. However, the evolution of the temperature and the electric field was not crucial in our modeling as long as the changes in thermodynamic state were successive. Indeed, as we applied a positive electric field, we only considered the positive solution of polarization of the free energy. Moreover, the Landau-Devonshire theory is independent of time and all thermodynamic changes are thermodynamically reversible. The model did not consider hysteresis and the frequency dependence of the material due to the underlying assumptions. The modeling represented a single Olsen cycle over a single ferroelectric domain independently of its size. Further work could be devoted to assessing the effect of waveforms and frequency on

the polarization and energy harvesting density. An electrical charge-discharge losses term added to the output energy was proposed by Smith *et al*[19]. Another possibility will be to use time-dependent Ginzburg-Landau (TDGL) model.

Energy harvesting can be more efficient if the thermodynamic conditions of the desired device are well established. Some studies aimed at improving the harvested energy by using phase transitions via modeling by phenomenological approach[19,20]. However, none of them made an investigation on using FE-FE phase transitions depending on the crystal orientation and the thermodynamic conditions. Here, we propose the optimum thermodynamic conditions for different ferroelectric crystals to perform Olsen's cycle with the help of such transitions. We decided to study different materials with temperature variation and electric field easily achievable for realistic applicative. The temperature variation $T_h - T_l$ has been chosen to be 10K as it is possible to have such a temperature variation in a short amount of time[21]. The electric field variation was set to $E_i = 0kV/mm$ and $E_f = 2kV/mm$. For studying energy harvesting in the frame of a thermodynamic approach, we modeled the thermodynamic path to represent the ideal energy harvesting cycle with Landau-Devonshire theory. The spontaneous polarization is obtained for each value of temperature and electric field and thus, the Olsen cycle can be obtained in the P-E space. An illustration of the Olsen cycle is presented on Fig. 1(a). The harvested energy is given by the hatched area of the P(E) cycle on Fig. 1(a) and can be expressed as:

$$W_h = \oint P(E)dE \tag{1}$$

III. MODEL

The Landau-Devonshire theory has been frequently investigated in for ferroelectrics but significantly less for energy harvesting purposes. In this work, we propose to study thermodynamic cycles and ferroelectric phase diagrams through the Landau theory for various ferroelectric materials and orientations. In the Landau-Devonshire theory, the free energy is developed as a function of an order parameter and must be symmetric by a point group of a reference phase. All the other terms that are added to the free energy (generally called second order parameters) must be also invariant by symmetry of the parent phase which is the m$\bar{3}$m (cubic) symmetry in our case[22,23]. The free energy is expressed as:

$$\begin{aligned} F_{lgd} &= F_0 + \alpha_{ij}P_iP_j + \alpha_{ijkl}P_iP_jP_kP_l + \alpha_{ijklmn}P_iP_jP_kP_lP_mP_n \\ &+ \alpha_{ijklmnop}P_iP_jP_kP_lP_mP_nP_oP_p + ... \end{aligned} \tag{2}$$

where P_i is the spontaneous polarization in the cubic basis; α_{ij}, α_{ijkl}, α_{ijklmn} and $\alpha_{ijklmnop}$ are tensors which represent the different orders of the dielectric stiffness and F_0 is the energy of the cubic phase (set to zero). In our study, only α_{ij} is temperature dependent and has a different expression depending on the studied material[24,25]. The different expressions are:

$$\alpha_{ij} = C * [\coth(\tfrac{T_s}{T}) - \coth(\tfrac{T_s}{T_c})] \tag{3}$$

and

$$\alpha_{ij} = C * (T - T_c) \tag{4}$$

where C is a constant, T_c is the Curie temperature and T_s is the saturation temperature. The dependence of α_{ij} with T_s makes it possible to describe the quantum effects that appear when T is less than T_s[26]. Unfortunately, finding this parameter for some ferroelectric perovskites is quite complex.

The total free energy for ferroelectric materials can be expressed as:

$$F = F_{lgd} + F_{elas} + F_{elec} + F_{grad} \tag{5}$$

F_{elas} and F_{grad} respectively represent the contribution to the free energy of an external stress and the different possible domains orientations of ferroelectric materials. Ginzburg first introduced the latter in the case of superconductivity[27]. In this study, we neglected these two terms as the crystal is in a stress-free condition, and a single crystal under a sufficient electric field can be considered in a single domain state[28]. Finally, only F_{lgd} and F_{elec} associated with the energy of an applied electric field have been considered. Under an external electric field, it is easier to express the energy in terms of free enthalpy variations instead of the free energy using the following equation (Legendre transformation):

$$\Delta G(P,T,E) = F_{lgd} - E_iP_i \tag{6}$$

With respect to the cubic O_h symmetry, the free enthalpy becomes:

$$\begin{aligned} \Delta G &= \alpha_1({P_1}^2 + {P_2}^2 + {P_3}^2) + \alpha_{11}({P_1}^4 + {P_2}^4 + {P_3}^4) \\ &+ \alpha_{12}({P_1}^2{P_2}^2 + {P_1}{P_3}^2 + {P_2}^2{P_3}^2) + \alpha_{123}{P_1}^2{P_2}^2{P_3}^2 \\ &+ \alpha_{111}({P_1}^6 + {P_2}^6 + {P_3}^6) + \alpha_{112}({P_1}^2({P_2}^4 + {P_3}^4) \\ &+ {P_2}^2({P_1}^4 + {P_3}^4) + {P_3}^2({P_1}^4 + {P_2}^4)) \\ &+ \alpha_{1111}({P_1}^8 + {P_2}^8 + {P_3}^8) \\ &+ \alpha_{1122}({P_1}^4{P_2}^4 + {P_1}^4{P_3}^4 + {P_2}^4{P_3}^4) \\ &+ \alpha_{1123}({P_1}^4{P_2}^2{P_3}^2 + {P_1}^2{P_2}^4{P_3}^2 + {P_1}^2{P_2}^2{P_3}^4) \\ &+ \alpha_{1112}({P_1}^6({P_2}^2 + {P_3}^2) + {P_2}^6({P_1}^2 + {P_3}^2) \\ &+ {P_3}^6({P_1}^2 + {P_2}^2)) - E_1P_1 - E_2P_2 - E_3P_3 \end{aligned} \tag{7}$$

where the E_i and P_i are the different components of the electric field and the polarization.

State	Polarization components	Number of configuration	Symmetry
Cubic	$(0,0,0)$	1	m$\bar{3}$m
Tetragonal	$(0,0,P)$	6	4mm
Orthorhombic	$(\frac{P}{\sqrt{2}},\frac{P}{\sqrt{2}},0)$	12	mm2
Rhombohedral	$(\frac{P}{\sqrt{3}},\frac{P}{\sqrt{3}},\frac{P}{\sqrt{3}})$	8	3m1

TABLE I. Properties of the different ferroelectric phases

Parameter	$BaTiO_3$[24,29]	PZN-4.5PT[30,31]	PMN-30PT[25,32]	Units
T_s	160	0	0	K
T_c	390	423.75	390.1	K
α_1	$5*10^5*T_s$ $\times[\coth(\frac{T_s}{T})-\coth(\frac{T_s}{T_c})]$	$1.9*10^5$ $\times(T-T_c)$	$6.22*10^4$ $\times(T-T_c)$	$V.m.C^{-1}$
α_{11}	$-1.154*10^8$	$-1.35*10^7$	$-1*10^8$	$V.m^5.C^{-3}$
α_{12}	$6.530*10^8$	$8.05*10^7$	$2*10^8$	$V.m^5.C^{-3}$
α_{111}	$-2.106*10^9$	$2.75*10^8$	$2.5*10^9$	$V.m^9.C^{-5}$
α_{112}	$4.091*10^9$	$4.125*10^8$	$-3.5*10^9$	$V.m^9.C^{-5}$
α_{123}	$-6.688*10^9$	$-2.14*10^9$	$-9*10^9$	$V.m^9.C^{-5}$
α_{1111}	$7.590*10^{10}$	0	$1*10^{10}$	$V.m^{13}.C^{-7}$
α_{1122}	$-2.221*10^{10}$	0	$8.6*10^{10}$	$V.m^{13}.C^{-7}$
α_{1112}	$-2.193*10^{10}$	0	$1*10^{10}$	$V.m^{13}.C^{-7}$
α_{1123}	$2.416*10^{10}$	0	$6.8*10^{10}$	$V.m^{13}.C^{-7}$
ρ	6.02	8.31	8	$g.cm^{-3}$
c	406	200	350	$J.kg^{-1}.K^{-1}$

TABLE II. List of Landau coefficients and physical properties

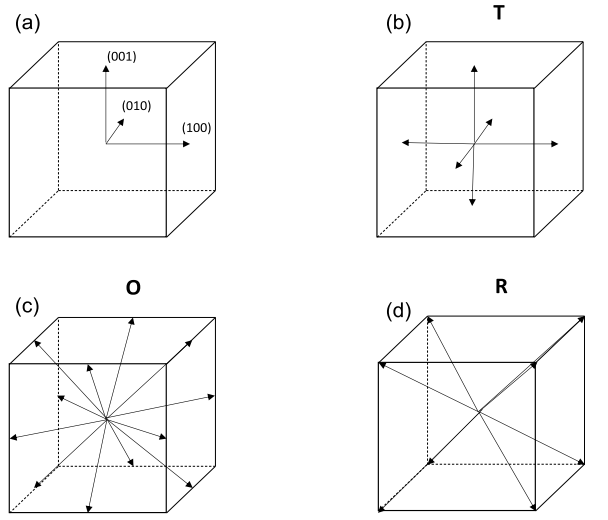

FIG. 2. The different possible orientations of the polarization for a ferroelectric crystal. (a) Referential of the cubic basis of the crystal; (b) Tetragonal phase with six possible orientations; (c) Orthorhombic with twelve possible polarization directions; (d) Rhombohedral and eight possible configurations.

By minimizing the free energy with respect to the polarization, we can find for each value of temperature and electric field the stable phase of the ferroelectric material and the associated polarizations. In our study, we consider four phases for each material. All the different ferroelectric states and polarization configurations are highlighted on Table I and are represented on Fig. 2.

The approach consisted in modeling thermodynamic cycles and to choose different values of low-temperature at which the cycle is started. We can identify the ideal zone for energy harvesting with variations of the initial temperature T_l. The main goal here is to use phase transition to increase the energy density. We choose to study $BaTiO_3$, PZN-4.5PT and PMN-30PT because they are one of the most studied ferroelectrics and there are a lot of available sets of Landau coefficients in the literature. Table II lists the Landau coefficients extracted from the literature for all the ferroelectric materials studied in this work. Depending on the crystal orientation, different ferroelectric phase transitions can be interesting. We choose here to consider the <001>,<011> and <111> crystallographic orientations. The electric field is applied along the cut direction as illustrated on Fig. 3. The free energy symmetry transformation is not necessary for <011> and <111> crystal orientation. In practice, the polarization is measured by the current variation flowing through the electrodes deposed on the faces in the electric field direction. Thus, the measured polarization is a projection of the polarization vector along the electric field direction. We therefore just changed the basis of the polarization vector[33,34] via a matrix rotation to this end. The polarization P' is defined in the basis of the laboratory reference frame (x',y',z') and the polarization P is defined in the cubic coordinate system (x,y,z), yielding:

$$P_i' = A_{ij}P_j \tag{8}$$

$$A_{ij}^{<001>} = \begin{pmatrix} 1 & 0 & 0 \\ 0 & 1 & 0 \\ 0 & 0 & 1 \end{pmatrix}$$

$$A_{ij}^{<011>} = \begin{pmatrix} 1 & 0 & 0 \\ 0 & \frac{1}{\sqrt{2}} & \frac{-1}{\sqrt{2}} \\ 0 & \frac{1}{\sqrt{2}} & \frac{1}{\sqrt{2}} \end{pmatrix} \tag{9}$$

$$A_{ij}^{<111>} = \begin{pmatrix} \frac{1}{\sqrt{2}} & \frac{-1}{\sqrt{2}} & 0 \\ \frac{1}{\sqrt{6}} & \frac{1}{\sqrt{6}} & \frac{-2}{\sqrt{6}} \\ \frac{1}{\sqrt{3}} & \frac{1}{\sqrt{3}} & \frac{1}{\sqrt{3}} \end{pmatrix}$$

We assume that the electric field is along the z' axis. Thus, we can define the unit vector $\vec{z'_{001}}$,$\vec{z'_{011}}$ and $\vec{z'_{111}}$and we can keep

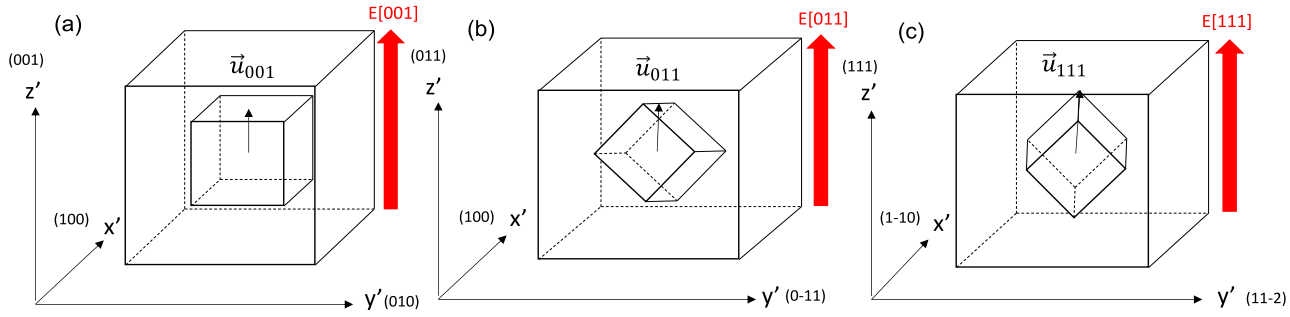

FIG. 3. Illustration of the crystal in the different orientations with the associates projection vector and basis. (a) <001> Orientation; (b) <011> orientation; (c) <111> orientation

.

using the cubic (m3m) symmetry free energy. The polarization along the crystal z' axis for different orientations is thus given by:

$$P_3'^{<001>} = \vec{P}.\vec{z'_{001}} \tag{10}$$

$$P_3'^{<011>} = \vec{P}.\vec{z'_{011}} \tag{11}$$

$$P_3'^{<111>} = \vec{P}.\vec{z'_{111}} \tag{12}$$

with respectively $\vec{z'_{001}} = (0,0,1)$, $\vec{z'_{011}} = (0, \frac{1}{\sqrt{2}}, \frac{1}{\sqrt{2}})$ and $\vec{z'_{111}} = (\frac{1}{\sqrt{3}}, \frac{1}{\sqrt{3}}, \frac{1}{\sqrt{3}})$

IV. ELECTROCALORIC EFFECT

In order to validate our approach, the electrocaloric effect of PMN-30PT and $BaTiO_3$ in different crystallographic orientations is assessed and compared to different studies in the litterature[35–38]. The electrocaloric effect is the ability of a material to change temperature when an electric field is applied. It is usually considered as the converse effect of pyroelectricity. We propose here to obtain the temperature variation via the converted energy in order to confirm the phenomenological approach to model Olsen cycle. Assuming the Maxwell relation $(\frac{\partial P}{\partial T})_E = (\frac{\partial S}{\partial E})_T$. It is possible to express the heat flow of the electrocaloric effect Q_{ECE} as:

$$Q_{ECE} = T_h \int_{E_i}^{E_f} pdE \tag{13}$$

where p is the pyroelectric coefficient The converted energy can be expressed depending on the pyroelectric coefficient as:

$$W_h = -(T_h - T_l) \int_{E_i}^{E_f} pdE \tag{14}$$

If we substitute equation (14) in equation (13) the converted energy yields:

$$W_h = -\eta_{carnot} Q_{ECE} \tag{15}$$

where $\eta_{carnot} = \frac{T_h - T_l}{T_h}$ is the Carnot's efficiency. Finally we can express the temperature difference of the electrocaloric effect as:

$$\Delta T_{ECE} = \frac{W_h}{\eta_{carnot} \rho c_p} \tag{16}$$

where ρ is the density of the material and c the specific heat. We can note that this equivalence depends on the temperature variation $T_h - T_l$. As we set this difference to 10K, it is a range of temperature where it is possible to linearize the pyroelectric coefficient and express the converted energy W_h as a function of the heat flow Q_{ECE}[32]. This approximation provides a good trend for the electrocaloric effect. However, this approximation does not give a reliable absolute value of the temperature variation of the electrocaloric effect because it depends on the chosen temperature variation $T_h - T_l$. This still allows validating the Landau Devonshire approach to model energy harvesting for different crystallographic orientations. In fact, the most important in the scope of this study is the trend and the relative temperature variation obtained with the phenomenological approach, which are in good agreement with experimental results.

Marathe *et al*[36] used first principle calculation for modeling the electrocaloric effect and performed experimental measurement with different crystallographic orientation on barium titanate. Our results shown in Figs. 4 and 5 agreed with both experiments and first principle calculations. Especially, a negative temperature variation occurs for $BaTiO_3$ in the <001> direction at the O-T transition at 270K as shown in Fig. 4(a). Moreover, the <001> cut orientation will also induce a more significant temperature variation for barium titanate at the T-C transition compared to the other orientations. This behavior also agrees with experimental and first principle modeling and gives a good order of temperature variation for the electrocaloric effect[36,39].

The results obtained on the PMN-30PT also agree with experiments performed on different orientations[38,40,41]. In fact, the <001> cut crystals still present a negative temperature variation but this time for the R-T transition which occurs approximately at 360K for PMN-30PT as shown in

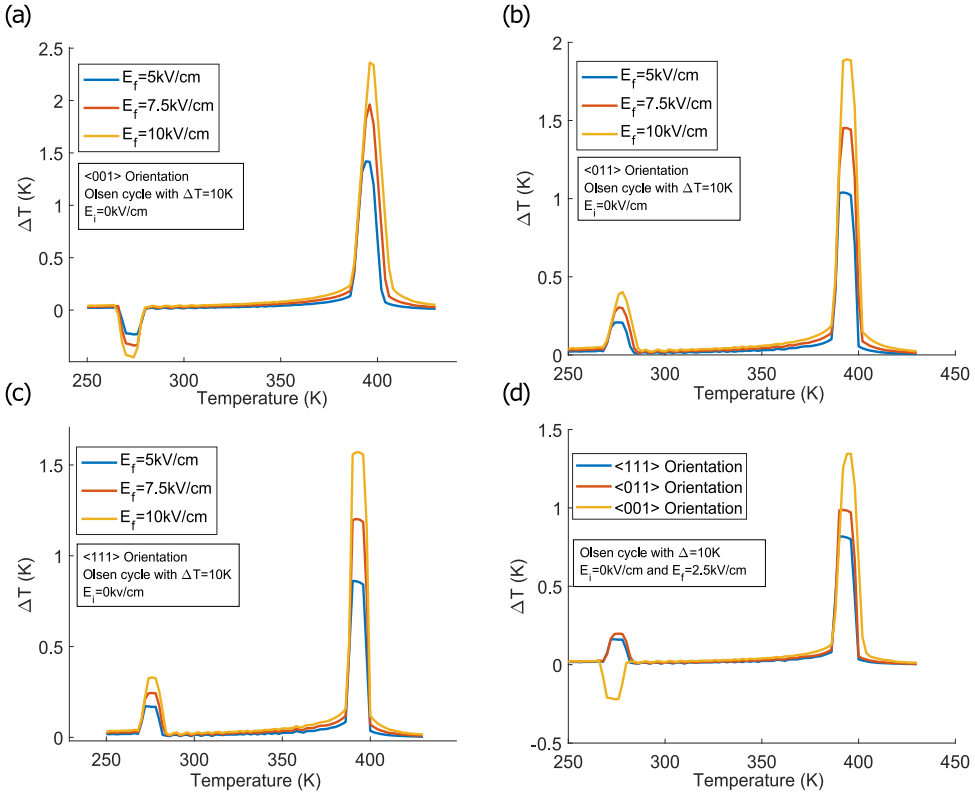

FIG. 4. Electrocaloric effect for $BaTiO_3$ in function of the temperature for different applied electric fields. (a) <001> orientation; (b) <011> orientation; (c) <111> orientation; (d) comparison between the three orientations.

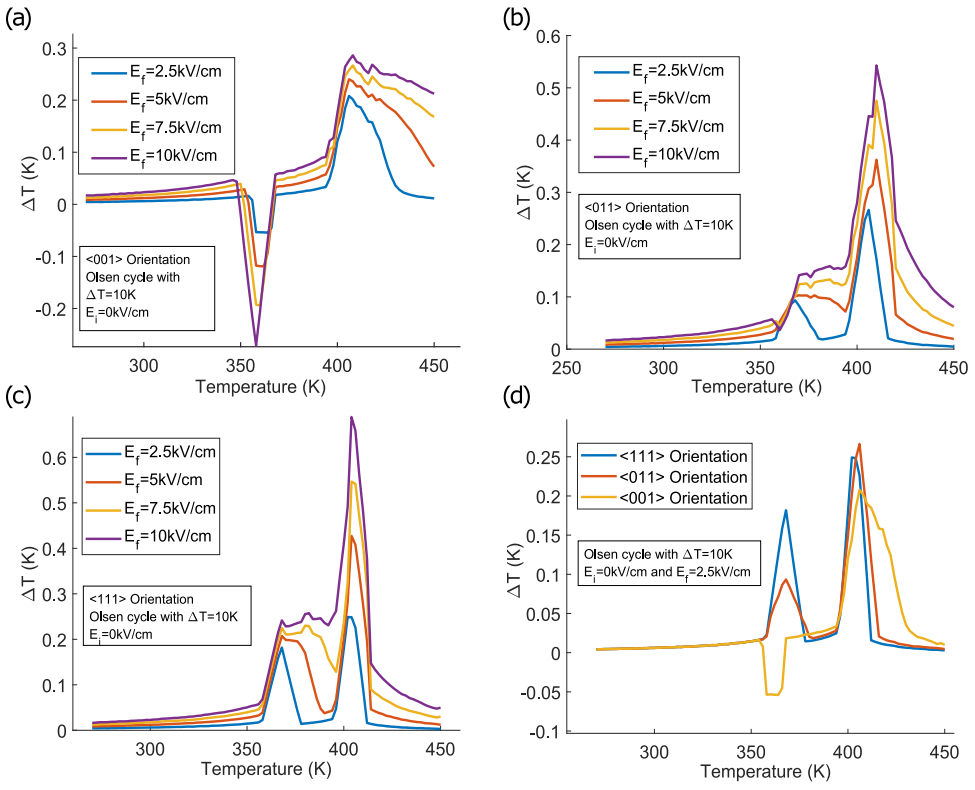

FIG. 5. Electrocaloric effect for PMN-30PT in function of the temperature for different applied electric fields. (a) <001> orientation; (b) <011> orientation; (c) <111> orientation; (d) comparison between the three orientations.

Fig. 5(a). These negative electrocaloric effects are due to the polarization that increases with temperature ($\frac{\partial P}{\partial T} > 0$). This phenomenon appears for specific FE-FE transitions in particular orientations. Compared to $BaTiO_3$, it is the <111> orientation for PMN-30PT that provides better temperature variations at the T-C transition. This result was already observed in the literature[38,42], thus giving an experimental confirmation of the phenomenological approach in the small temperature variation regime. Particularly, it predicts which FE-FE presents negative or positive peak in particular crystal orientation for specific phase transition of ferroelectric materials. These results therefore explain negative electrocaloric effect due to crystal orientation with Landau-Devonshire theory.

Both materials had an electrocaloric temperature variation which evolves monotonously with increasing electric field. Also, the electric field shifts the temperature of the peak. This temperature shift could be positive or negative depending on both crystal orientation and applied electric field direction. It can be observed that negative electrocaloric peaks associated with FE-FE transitions shift negatively with temperature for <001> orientation of $BaTiO_3$ and PMN-30PT in Fig. 4(a) and Fig. 5(a). These transitions correspond respectively to the O-T and the R-T transition. The positive electrocaloric peaks, on the contrary, are associated with a positive temperature shift with an increasing electric field for all FE-FE transitions of <011> and <111> crystal orientation, as shown in Fig. 4(d) and Fig. 5(d). Moreover, all orientations have a positive shift for electrocaloric peaks associated with the T-C transition. This behavior is due to the electric field, which favors the ferroelectric phase energetically compared to the paraelectric one. Another feature of both materials is a wider maximum peak when the electric field is smaller. This phenomenon can be well observed in Fig. 5(a) on the R-T transition at 370K. This result originates from the equivalence made between the harvested energy and the electrocaloric effect and has no real significance for the electrocaloric effect. This emphasizes the limitation of the approximation of equation (15) as an arbitrary temperature variation needed to be fixed for the Olsen cycle (10K here).

V. ENERGY HARVESTING

This section is devoted to the simulation method and the comparison of the Olsen cycle predicted and measured harvested energy. We will still consider PMN-30PT and $BaTiO_3$ with the three orientations detailed before. We choose to model the harvested energy as a function of the low temperature T_l while keeping a temperature span of $\Delta T = T_h - T_l = 10K$, $E_i = 0kV/cm$ and $E_f = 2kV/mm$ (Fig. 6(a),(d) and (g) and Fig. 7(a),(d) and (g)). These settings allows selecting the best working temperature range to improve the output energy of pyroelectric materials via phase transitions. We identified different typical values of energy that we denote with different numbers. These numbers are associated with thermodynamic cycles represented in a T-E phase diagram in Fig. 6(b),(e) and (h) and Fig. 7(b),(e) and (h). We also represented the associated cycles in the P-E space in Fig. 6(c),(f) and (i) and Fig. 7(c),(f) and (i).

The PMN-30PT in the <001> orientation depicted in Fig. 6(a),(b) and (c). A negative energy peak arises at $T_l = 346K$ for cycle n°1. This negative peek is associated with the R-T transition which occurs during the temperature variation at a constant electric field of $E_f = 2kV/mm$. When we decrease the electric field, the material returns to its initial rhombohedral state. These different phase transitions result in an anticlockwise cycle in the high electric field region. Hence, this yields an energy loss or a minimal harvested energy in practical conditions.

For the <011> orientation of PMN-30PT in Fig. 6(d),(e) and (f), cycle n°1 also presents a negative peak at $T_l = 360K$. This negative peak is due to the R-O transition. This transition happens during the heating in the isoelectric process and induces an increase of polarization due to the orthorhombic state favorable orientation. As for PMN-30PT <001>, we still have an anticlockwise cycle in the high electric field region. However, this energy loss is compensated by an energy gain in the low electric field region due to successive O-R and R-T transitions.

In the <111> orientation (Fig. 6(g),(h) and (i)), we have a positive energy peak at $T_l = 366K$ which corresponds to a temperature slightly lower than the R-T temperature transition at $E_i = 0kV/mm$. Cycle n°1 is fully clockwise compared to the orientations. The harvested energy arises due to the occurence of the R-T transition at the high temperature T_h when we release the electric field. This transition induces a fast polarization decrease. Hence, the area of the cycle is increased and therefore, energy is effectively harvested. During the cooling of the material, the <111> PMN-30PT transits back to the rhombohedral structure.

For all the PMN-30PT different orientations, cycle n°2 is the most interesting in terms of energy gain and of course made profit of the T-C transition due to the larger polarization variation at the Curie temperature. In all cases, it is always better to start the cycle with T_l being close to the Curie temperature T_c. Performing the cycle at T_l just before the Curie temperature increases the area of the thermodynamic cycle. It is the $< 111 >$ orientation which gives the highest harvested energy compared to the others. This is due to the T-C transition that occurs at a higher value of electric field for the <111> orientation. It is noteworthy that the <001> orientation has the highest value of polarization for the tetragonal phase. We would thus expect it to be the best orientation to work at T_c as it is possible to have larger polarization variations. However, it is the one who gave the less energy output. This is due to the significant shift of the Curie temperature T_c with the electric field maintaining a ferroelectric state at high temperature and small electric field.

Barium titanate exhibits different results. In <001> orientation (Fig. 7(a),(b) and (c)), both R-O and O-T transitions present negative energy peaks respectively at $T_l = 195K$ and

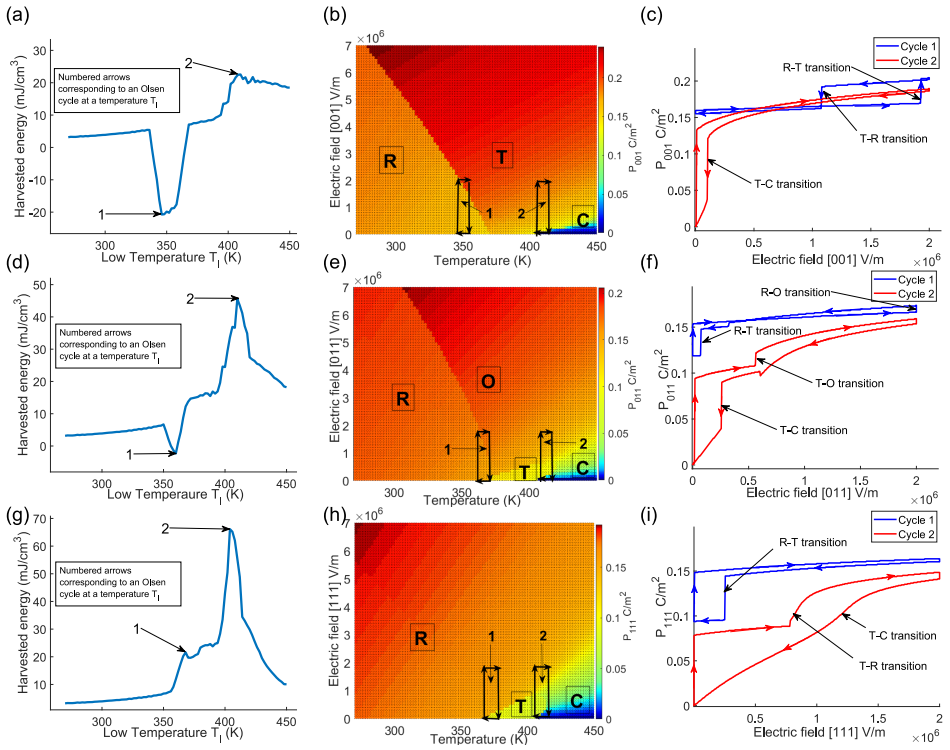

FIG. 6. A plot of the harvested energy in function of the working temperature T_l for PMN-30PT. (a) <001> orientation; (d) <011> orientation; (g) <111> orientation. Temperature-Electric field phase diagram versus polarization for PMN-30PT. (b) <001> orientation; (e) <011> orientation; (h) <111> orientation. A plot of the associated P(E) cycles for PMN-30PT. (c) <001> orientation; (f) <011> orientation; (i) <111> orientation.

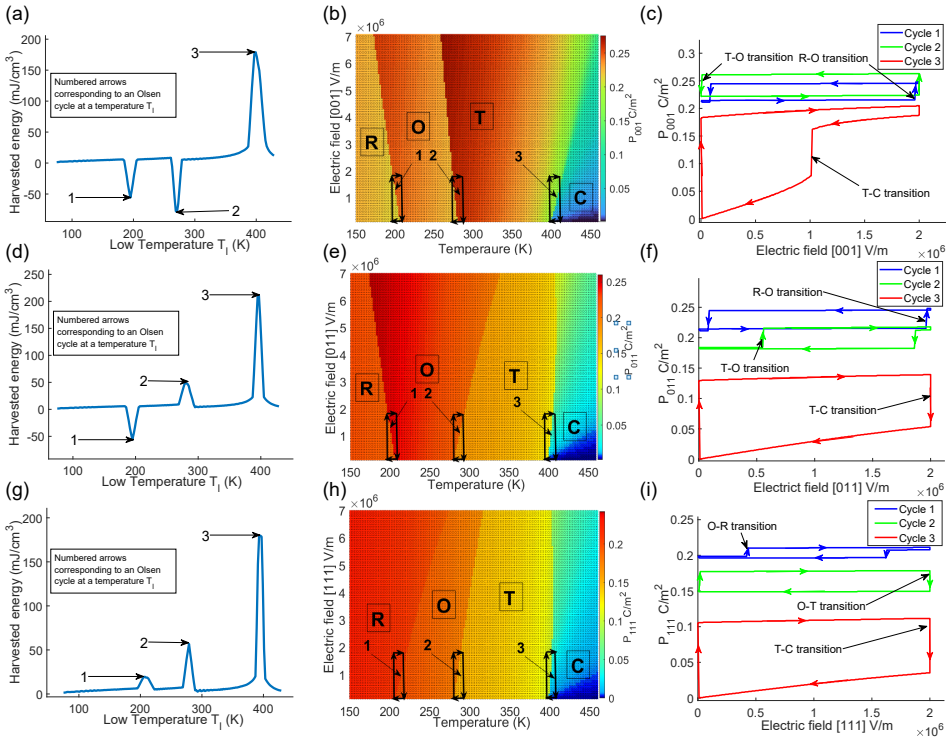

FIG. 7. A plot of the harvested energy in function of the working temperature T_l for $BaTiO_3$. (a) <001> orientation; (d) <011> orientation; (g) <111> orientation. Temperature-Electric field phase diagram versus polarization for $BaTiO_3$. (b) <001> orientation; (e) <011> orientation; (h) <111> orientation. A plot of the associated P(E) cycles for $BaTiO_3$. (c) <001> orientation; (f) <011> orientation; (i) <111> orientation.

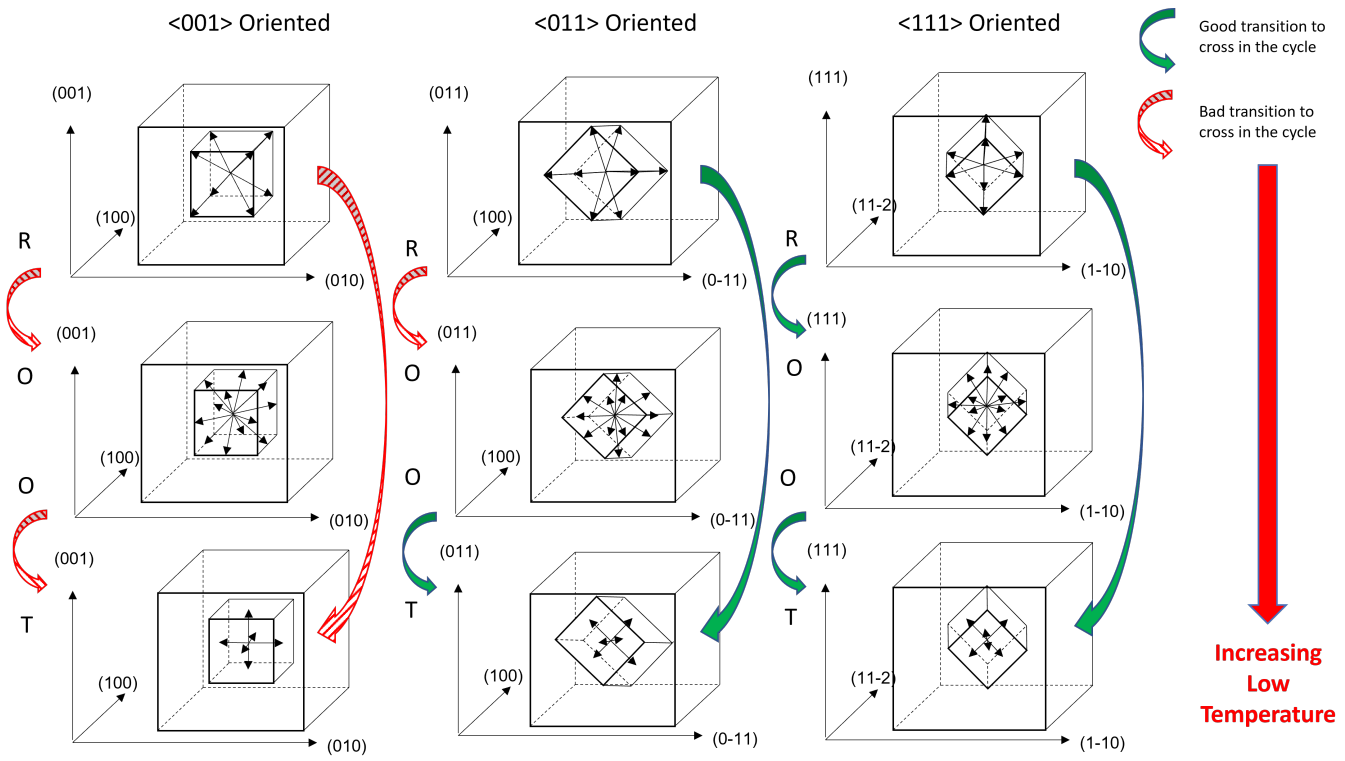

FIG. 8. Illustration of the different phase transitions possible for different crystal orientations.

$T_l = 269K$. Peak n°2 associated with cycle n°2 is larger than n°1. This behavior comes from the significant increase of polarization in the O-T transition compared to the R-O one. Both transitions happen during heating in the isoelectric process and they both have an anticlockwise rotation cycle.

In the <011> orientation (Fig. 7(d),(e) and (f)), peak n°1 and cycle n°1 at $T_l = 195K$ exhibits the same behavior as the <001> orientation. However, cycle n°2 at $T_l = 282K$ is favorable for energy harvesting. This time the O-T transition corresponds to a decrease of polarization. Another point is the low temperature T_l which is optimum just before the O-T transition at zero field.

All of the FE-FE transitions for the <111> oriented $BaTiO_3$ are of interest and presents positive energy peaks. Cycle n°1 and n°2 present a lower value of temperature respectively of $T_l = 209K$ and $279K$ and both are situated just before the FE-FE transition without the application of the electric field. Cycle n°2 is better in term of energy gain as the O-T transition shows a larger polarization variation.

For barium titanate, the Curie temperature region also remains the most interesting region to exploit for pyroelectric energy harvesting purpose. Cycle n°3 for the <001> and <111> orientations exhibits an energy density of $190mJ/cm^3$ whereas for the <011> the value is almost $220mJ/cm^3$. As for the PMN-30PT, for all orientations the energy peak n°3 is located at a temperature T_l just before T_c. For the <001> orientation, the polarization variation is more important but the Curie temperature shifts more with respect to the electric field compared to other orientations. The fact that $\frac{\partial T_c}{\partial E}$ is more important for the <001> oriented crystal does not allow the T-C transition to occur during the heating in the isoelectric process for a temperature variation of $T_h - T_l = 10K$. The transition appears only when we release the electric field whereas for the <011> and <111> orientations, the FE-PA happens during heating but the polarization variation is smaller. So the area of the cycle, and thus the harvested energy, is a trade-off between favorable crystal orientation and Curie temperature shift, the best being a <001> ferroelectric oriented crystal with a weak Curie temperature shift. Additionally, we can note that when the temperature of a FE-FE transition shift positively with the electric field, then the energy density is positive and favors energy harvesting. On the contrary, when this shift is negative, the energy density is negative, leading to an unfavorable temperature window for pyroelectric energy harvesting.

Fig. 8 displays a summary of the optimum phase transitions for pyroelectric energy harvesting with respect to their crystal orientations. To compare our model with experimental results, a plot of the harvested energy depending on the temperature variation is proposed on Fig. 9. In this comparison, T_l is set to be constant at 373K. The experiment was performed by Khodayari *et al*[43] on <011> oriented PZN-4.5PT with an applied electric field along the [011] direction. To determined the landau coefficients of PZN-4.5PT, we used a linear composition law with the coefficient of PZN and PT[31]

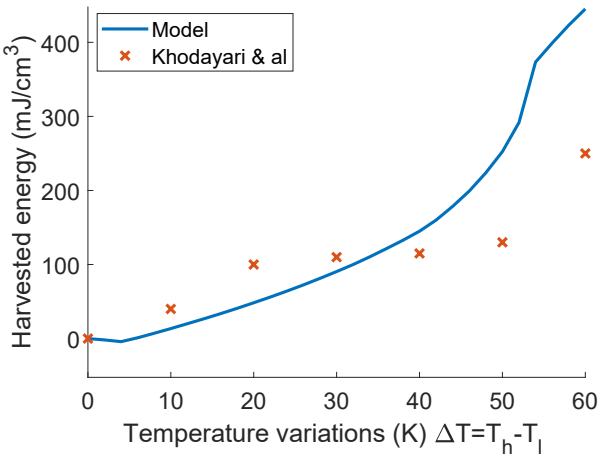

FIG. 9. A plot of the harvested energy in function of the temperature variation $T_h - T_l$ for an Olsen cycle with $E_i = 0kV/mm$ and $E_f = 2kV/mm$ for a <011> oriented single crystal of PZN-4.5PT and an electric field applied in the [110] direction.

One can notice that the harvested energy predicted by the model is close to the measured one. The trend of the curve is also fine. A fast increase of the energy occurs for $\Delta T = 60K$ in both curves due to the T-C transition. However, the fitting is not perfect and these differences can be explained by the presence of Polar Nano Regions (PNRs) especially in the high temperature region close to the Burns temperature. These PNRs give other contributions to the intrisic polarization[44]. We also made the assumption that we had a single domain crystal which is not the case in a real experiment. There are multiple domains, domain wall motions are induced which modify the polarization response. However, as we consider sufficient applied electric field, our hypothesis remains rather valid. Finally, the electrical losses occurring during the charging and discharging process are ignored in our modeling.

VI. CONCLUSION

In this study, we investigated the influence of crystal orientation for different ferroelectric perovskites material in order to identify the best phase transitions for optimizing the pyroelectric energy harvesting using Olsen cycles. An important additional feature of this work was to explain the negative electrocaloric peaks with the equivalence between pyroelectric energy harvested and electrocaloric effect. It is the first study in our knowledge to obtain such behavior with phenomenological approach. Moreover, a good agreement in term of order of magnitude and temperature values for the electrocaloric peaks has been obtained. The other highlight of this article is to model Olsen's cycle with Landau-Devonshire theory to predict the best thermodynamic conditions to realize realistic pyroelectric harvester devices. In all cases, the FE-PA transition maximizes pyroelectric energy harvesting. The FE-FE transitions can improve the energy density for particular orientations and electric field. On the contrary, other orientations can decrease the energy density by using FE-FE transitions. For some materials and applications, it is complicated to work in the Curie temperature region (100°C). While being of lower energy density compared to FE-PA transition, taking profit of FE-FE transitions could be a good alternative to increase the output energy. We demonstrated it is better to use <011> orientation and the O-T transition or the <111> orientation with the R-O and the O-T transitions for Olsen cycle. The R-O transition in a <011> oriented crystal and all the FE-FE transitions for a <001> crystal orientations will reduce the harvested energy. These results are true in the frame of a classical Olsen thermodynamic cycle. Of course, working close to the Curie temperature is still the best option for such applications. We have nevertheless shown that for this purpose, the ideal ferroelectric material will be in the <001> orientation with a small shift of the Curie temperature with electric field. This result emphasizes the point that when a transition is favorable, the ideal low temperature (T_l) is slightly before the temperature transition. Moreover, most of ferroelectric materials are solid solutions and change their temperature transitions by changing their mixing proportions. Thus, it is possible to tailor a composition to have a cycle with a low temperature (T_l) at the ambient temperature, while, made profit of the favorable phase transitions of specifics crystal orientation identified in this study. The ideal cycle would cross the transition during the heating and cross the transition back during the cooling process. Finally, the predicted energy harvested is of good magnitude and trend vs. the working temperatures. However, some discrepancies still occurs between modeling and experiments. These difference can be explained by several mechanisms. First of all, the Landau-Devonshire theory considers only a single ferroelectric domain. Secondly, there are always electrical losses when applying or releasing electric field. Another difference with a real experiment is the hysteresis with ferroelectrics. Even though the Landau-Devonshire theory can reproduce the coercive electric field, there is always hysteresis in ferroelectrics and the experimental results necessarily depend on the history of the material. Finally, in ferroelectric relaxors such as xPMN-$(1-x)$PT and xPZN-$(1-x)$PT, PNRs regions appears and give other contributions to the polarization. All of these contributions can be a basis for further investigations. To conclude, phenomenological approach can be useful to identify interesting thermodynamic regions and benefiting of phase transitions for real optimized energy harvesting devices.

ACKNOWLEDGMENTS

This work was performed under the framework of the ANR-FIESTA project, funded by the French Agence Nationale pour la Recherche, grant ANR-20-CE05-0026, and under the framework of the International Research Network ELyT Global.

AUTHOR DECLARATIONS

CONFLICT OF INTEREST

The authors have no conflicts to disclose.

DATA AVAILABILITY STATEMENT

The data that support the findings of this study are available from the corresponding author upon reasonable request.

REFERENCES

[1] L. Livermore, "U.s. energy flow trends - 2012," (2013).
[2] I. M. McKinley, *Thermomechanical Energy Conversion Using Ferroelectric Materials*, Ph.D. thesis, UCLA (2013).
[3] A. Sultana, M. M. Alam, T. R. Middya, and D. Mandal, Applied Energy **221**, 299–307 (2018).
[4] H. A. Sodano, G. E. Simmers, R. Dereux, and D. J. Inman, Journal of Intelligent Material Systems and Structures **18**, 3–10 (2007).
[5] S. Pandya, G. Velarde, L. Zhang, J. Wilbur, A. Smith, B. Hanrahan, C. Dames, and L. Martin, NPG Asia Materials **11**, 26 (2019).
[6] D. Guyomar, A. Badel, E. Lefeuvre, and C. Richard, IEEE Transactions on Ultrasonics, Ferroelectrics, and Frequency Control **52**, 584 (2005).
[7] M. Lallart and G. Lombardi, Energy Conversion and Management **203**, 112135 (2020).
[8] N. Sharpes, D. Vučković, and S. Priya, Energy Harvesting and Systems **3**, 43 (2016).
[9] X. Xu, D. Cao, H. Yang, and M. He, International Journal of Pavement Research and Technology **11**, 388 (2018).
[10] D. Guyomar, S. Pruvost, and G. Sebald, IEEE Transactions on Ultrasonics, Ferroelectrics, and Frequency Control **55**, 279 (2008).
[11] R. Kandilian, A. Navid, and L. Pilon, Smart Materials and Structures **20**, 055020 (2011).
[12] D. Blankschtein and R. M. Hornreich, Phys. Rev. B , 3214 (1985).
[13] K. M. Rabe, K. M. Rabe, C. H. Ahn, and J.-M. Triscone, *Physics of Ferroelectrics: A Modern Perspective* (Springer Publishing Company, Incorporated, 2007).
[14] A. Devonshire, "Xcvi. theory of barium titanate," **40**, 1040 (1949).
[15] R. B. Olsen, D. A. Bruno, and J. M. Briscoe, Journal of Applied Physics **58**, 4709 (1985).
[16] B. Hanrahan, C. Mart, T. Kämpfe, M. Czernohorsky, W. Weinreich, and A. Smith, Energy Technology **7**, 1900515 (2019).
[17] S. Pandya, J. Wilbur, J. Kim, R. Gao, A. Dasgupta, C. Dames, and L. Martin, Nature Materials, **17** (2018).
[18] B. Bhatia, A. R. Damodaran, H. Cho, L. W. Martin, and W. P. King, Journal of Applied Physics **116**, 194509 (2014).
[19] A. N. Smith and B. M. Hanrahan, Journal of Applied Physics **128**, 024103 (2020).
[20] F. Zhuo, Q. Li, Y. Li, J. Gao, Q. Yan, Y. Zhang, X. Xi, X. Chu, and W. Cao, Journal of Applied Physics **121**, 064104 (2017).
[21] A. Sharma, M. Behera, D. Pradhan, S. Pradhan, C. Bonner, and M. Bahoura, Scientific Reports **11**, 111 (2021).
[22] W. Cao, Ferroelectrics **375**, 28 (2008).
[23] J.-Y. Li, C. H. Lei, L.-J. Li, Y.-C. Shu, and Y. Liu, Acta Mechanica Sinica **28** (2012).
[24] J. J. Wang, P. P. Wu, X. Q. Ma, and L. Q. Chen, Journal of Applied Physics **108**, 114105 (2010).
[25] J. H. Qiu, J. N. Ding, N. Y. Yuan, and X. Q. Wang, Journal of Applied Physics **117**, 074101 (2015).
[26] E. K. H. Salje, H. Zhang, D. Schryvers, and B. Bartova, Applied Physics Letters **90**, 221903 (2007).
[27] V. L. Ginzburg and L. D. Landau, "On the theory of superconductivity," in *On Superconductivity and Superfluidity: A Scientific Autobiography* (Springer Berlin Heidelberg, 2009) p. 113.
[28] P. Chandra and P. B. Littlewood, "A landau primer for ferroelectrics," in *Physics of Ferroelectrics: A Modern Perspective* (Springer Berlin Heidelberg, 2007) p. 69.
[29] Y. He, Thermochimica Acta **419**, 135 (2004).
[30] M. A. Hamad, Phase Transitions **86**, 307 (2013).
[31] K. Abe, O. Furukawa, and H. Imagawa, Ferroelectrics **87**, 55 (1988).
[32] G. Sebald, S. Pruvost, and D. Guyomar, Smart Materials and Structures **17**, 015012 (2007).
[33] H. Zhang, Y. Feng, Y. Wang, Y. Tang, Y. Zhu, and X. Ma, Acta Materialia **228**, 117761 (2022).
[34] X. Guo, M. Zou, Y. Wang, Y. Tang, Y. Zhu, and X. Ma, Acta Materialia **206**, 116639 (2021).
[35] R. Chukka, S. Vandrangi, Z. Chen, L. You, J. Wang, P. Yang, and L. Chen, AIP Advances **3**, 072118 (2013).
[36] M. Marathe, D. Renggli, M. Sanlialp, M. O. Karabasov, V. V. Shvartsman, D. C. Lupascu, A. Grünebohm, and C. Ederer, Phys. Rev. B **96**, 014102 (2017).
[37] Q. Jian-Hua, W. Xiu-Qin, N. Yuan, and D. Jian-Ning, Communications in Theoretical Physics **64** (2015).
[38] J. Li, R. Yin, X. Su, H.-H. Wu, J. Li, S. Qin, S. Sun, J. Chen, Y. Su, L. Qiao, D. Guo, and Y. Bai, Acta Materialia **182**, 250 (2020).
[39] Z. Li, J. Li, H.-H. Wu, J. Li, S. Wang, S. Qin, Y. Su, L. Qiao, D. Guo, and Y. Bai, Acta Materialia **191**, 13 (2020).
[40] F. Le Goupil, A. Berenov, A.-K. Axelsson, M. Valant, and N. Alford, Journal of Applied Physics **111**, 124109 (2012).
[41] J. Peräntie, J. Hagberg, A. Uusimäki, and H. Jantunen, Phys. Rev. B **82**, 134119 (2010).
[42] Y. Bai, D. Wei, and L.-J. Qiao, Applied Physics Letters **107**, 192904 (2015).
[43] A. Khodayari, S. Pruvost, G. Sebald, D. Guyomar, and S. Mohammadi, IEEE Transactions on Ultrasonics, Ferroelectrics, and Frequency Control **56**, 693 (2009).
[44] H. Li, H. Tian, D. Gong, Q. Meng, and Z. Zhou, Journal of Applied Physics **114**, 054103 (2013).